*06*

# Microstructure and properties of polycrystalline diamond coatings synthesized by HFCVD at high methane concentrations

© A.S. Mitulinsky, A.V. Gaydaychuk, S.P. Zenkin, V.A. Bulakh, S.A. Linnik

Tomsk Polytechnic University, Tomsk, Russia
e-mail: mitulinsky@tpu.ru

In this paper we present the results of experimental studies of the dependence of the structure and mechanical properties of diamond films grown by HFCVD method in an $H_2/CH_4$ atmosphere on variations in the methane concentration (from 5.6 to 19.3 vol.%). Films synthesized at 5.6 vol.% $CH_4$ have a columnar microcrystalline structure. The microstructure of films grown at high methane contents ($12.2-19.3$ vol.%) contains both individual diamond crystals and dendritic clusters, the calculated values of the crystal sizes of such films are $\sim 5$ nm. Depending on the deposition parameters, the hardness and elastic modulus of diamond films varied from 50.4 and 520 GPa to 95.15 and 974.5 GPa, respectively. With an increase in the $CH_4$ concentration during deposition, an increase in residual tensile stresses occurs. In addition, the dependence of residual stresses on the film thickness is presented. Ultrananocrystalline coatings have, on average, order of magnitude lower values of surface roughness than microcrystalline ones; in all films, an increase in roughness is observed with an increase in their thickness.

**Keywords:** thin films, chemical vapor deposition, ultrananocrystalline diamond.

DOI: 10.61011/TP.2023.06.56528.2-23

## Introduction

Diamond is a material with outstanding physical and mechanical properties [1–6]. Due to the combination of high hardness and wear resistance, high thermal conductivity and low coefficient of friction the diamond coatings are used to protect the surfaces of various products subjected to intense abrasive wear, such as, for example, cutting tools [7–9] and end-face seals [10,11]. Such coatings are also used in microelectromechanical systems, biomedicine, etc. [12].

Diamond films are synthesized by CVD method. There are different variations of this method, the most common of which are hot filament CVD (HFCVD) and microwave plasma CVD (MPCVD). To modify the structure of diamond CVD films, various approaches are used, including changing the concentration of carbon-containing gas composition in the working mixture, changing the working gas, for example, adding argon, nitrogen, etc., changing the pressure in the reactor and the substrate temperature [13–17]. According to their structure the diamond films are divided into microcrystalline diamond (MCD) (grain size larger than $1\,\mu m$), submicrocrystalline (SMCD) (from 100 nm to $1\,\mu m$), nanocrystalline (NCD) (from 10 to 100 nm) and ultrananocrystalline (UNCD) (less than 10 nm). Currently, ultrananocrystalline structures are of the greatest interest for study due to their extremely low grain size, which leads to a significant change in surface morphology, redistribution of internal stresses, and changes in physical, mechanical and electrical properties [17–20]. Numerous studies indicate a decrease in the hardness and modulus of elasticity of films with the grain size decreasing [19,21], however, there are also opposite data, for example, paper [22] reported

the hardness and modulus of elasticity of UNCD equal to 98 and 980 GPa, respectively. A number of papers indicate that the surface roughness and friction coefficient of diamond films decrease with the size decreasing of the diamond grains. It is also said that the surface roughness of UNCD films is independent of their thickness, which distinguishes them from other polycrystalline diamond structures, in which the roughness increases with film thickness increasing. There is inconsistency in the data on the level of residual stresses in films of various types. The paper [26] reports on higher residual compression stresses in UNCD films than in MCD and NCD films; and on other hand, papers [20,27] report on decrease in compression residual stresses in UNCD films. The number of papers, in which it is possible to trace the dynamics of the properties of specifically UNCD films dependence on the deposition parameters, is extremely limited. The paper [26] presents the dynamics of the properties of UNCD films with variations in the working pressure during deposition (from 6 to 24 Torr) for methane contents of 10 and 14% in the atmosphere $H_2/CH_4/Ar$. In the majority of papers UNCD films were deposited at rather low concentrations of $CH_4$ ($1-10\%$) [19,23,28,29]. In the paper [30] the dynamics of changes in the structure of the synthesized coatings at high methane concentrations ($0.5-40\%$ $CH_4$) was studied, but change in the properties of the films was not considered. The effect of high methane concentrations upon deposition in methanehydrogen atmosphere on the properties of diamond UNCD films requires further study.

There is also ambiguity in the structural characterization of UNCD coatings. In many papers [31,32] their typical structure is presented as a system of randomly oriented

nanosized diamond crystallites, densely and uniformly distributed throughout the entire volume of the film, implying that in the process of film growth the constant renucleation occurs, leading to homogeneous grain sizes. At the same time, other papers indicate that in an atmosphere with nitrogen addition a structure is formed, consisting of nanosized crystalline diamond clusters, called „needle-like" [33–35]. It is worth noting that „needle-like" structure is also observed in diamond films grown in an atmosphere of $H_2/CH_4$ without nitrogen [29]. Another feature of the growth of UNCD films is the tendency to the formation of spherical crystalline agglomerations, which are observed both at the initial stages of film growth and on the surface of films with thickness over $5\,\mu m$ [26,36.37]. The formation of such agglomerations indicates some type of vertical bonds in the bulk of the UNCD films. In the papers [38,39] by thermal oxidation of the diamond film the authors showed that in addition to the dense structure of small diamond grains, the growth of microsized crystals and the formation of dendritic clusters are observed in UNCD films. Besides, in paper [40] as a result of electrochemical etching of UNCD the dendritic structure of diamond clusters was discovered, which the authors called „diamond nanofeathers". These data also indicate vertical relationships in UNCD films. Thus, the evolution of the growth of UNCD and NCD films, as well as the differences in their microstructure, were not yet explicitly determined (despite many years of studies), which makes further studies in this direction important.

The aim of this paper was to systematically study the dependence of the microstructure and a number of properties of diamond films synthesized by the classical HFCVD method on the concentration of carbon-containing gas in the working mixture $H_2/CH_4$. For this the series of samples with MCD and UNCD structures were synthesized, studies were carried out using Raman spectroscopy, X-ray diffraction analysis, the structure was characterized by SEM and TEM methods, the hardness, modulus of elasticity, and surface roughness of the samples were measured, and residual stresses were calculated.

## 1. Experimental methods and results processing

Diamond coatings were synthesized on silicon (100) substrates with dimensions of $5 \times 30 \times 0.38$ mm. The substrates were prepared for the deposition process as follows: primary cleaning with acetone in an ultrasonic bath, duration 10 min, „seeding" diamond growth centers with an aqueous solution of nanodiamond particles in the ultrasonic bath, duration 5 min, repeated cleaning with acetone in the ultrasonic bath, duration 5 min. „seeding" is carried out in order to increase the density of growth centers to achieve the uniformity of the synthesized films.

Synthesis of diamond films was carried out by the method of hot filament chemical vapor deposition (HFCVD). A mixture of methane-hydrogen in various concentrations was

used as working gas, while the hydrogen flow remained constant at 100 ml/min. For the microcrystalline films synthesis, the methane concentration was 5.6 vol.%, and for films with ultrananocrystalline structure the methane concentration was 12.2, 15.9, and 19.3 vol.%. The pressure in the chamber was maintained at a level of $20\pm1$ Torr. Gases flow monitoring was carried out using El-Flow (Bronkhorst) gas mass flowmeters. The temperature of the substrates during the experiments was maintained at $850\pm20\,°$C.

The microstructure and surface of the coatings were analyzed by the following methods: scanning electron microscopy (JSM-7500F, JEOL), atomic force microscopy (NTGRA, NT-MDT), transmission electron microscopy (JEM-2100F, JEOL), and Raman spectroscopy (NanoScan Technology Centaur IHR with 514.5 nm argon ion laser). Electron microscopy was performed using the equipment of the Center for Collective Use of NMNT TPU (supported by the project of the Ministry of Education and Science of Russia № 075−15−2021−710).

The phase purity of the synthesized films was studied by X-ray diffraction analysis (XRD) in the grazing beam mode $(5°)$ using $CuK_\alpha-$ radiation $(\lambda = 0.154$ nm) on a Shimadzu XRD 6000 X-ray diffractometer.

To estimate the residual stresses in the synthesized coatings, the Stoney equation was used, which includes the parameters of the coating and substrate, as well as the radius of curvature of the sample surface before and after deposition. The curvature radii were measured with a MICRO MEASURE 3D station (STILL) optical profilometer.

Hardness and modulus of elasticity were measured with a nanoindenter G200 (MTS-Agilent). All measurements were carried out under a load of 30 mN, 10 measurements were made for each sample.

## 2. Results and discussion

Table shows the resulting coatings and their designations. Synthesized diamond films are characterized by two structural states: microcrystalline for MCD films, and nanocrystalline (without pronounced crystallinity observed in SEM images) for films D1−D3 (Fig. 1). The structural transition is determined by the following. Atomic hydrogen in the gas mixture, which etches predominantly non-diamond phases, at high concentrations also etches the diamond $sp^3-$ phase of carbon, albeit at a much lower

Synthesized coatings and their designations

| Name | Methane concentration, vol.% | Thickness, $\mu m$ |
|------|------------------------------|--------------------|
| MCD  | 5.6                          |                    |
| D1   | 12.2                         | $5-11$             |
| D2   | 15.9                         |                    |
| D3   | 19.3                         |                    |
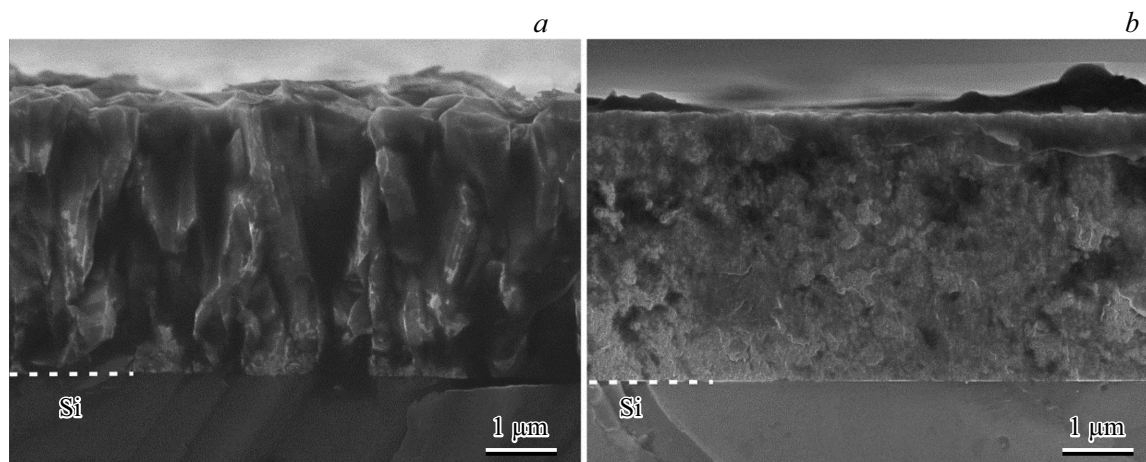
**Figure 1.** SEM images of the cross sections of films synthesized at 5.6 vol.% $CH_4$ (MCD) (*a*) and at 12.2 vol.% $CH_4$ (D1) (*b*).

rate, which leads to a decrease in the density of diamond crystals nucleation and contributes to the growth of large grains with a columnar morphology. With an increase in the methane concentration in the mixture $CH_4/H_2$, the hydrogen etching rate decreases, which leads to the increase in the rate of formation and growth of non-diamond phases at grain boundaries, the increase in the density of diamond nucleation, and consequently, to the decrease in the size of crystals.

Films with the microcrystalline structure have a characteristic columnar mechanism of diamond grain growth. This growth model is observed in many polycrystalline materials, it was described in the paper [41] and named „evolutionary selection". The essence of this phenomenon is that grains with a higher vertical growth rate (with a preferred orientation) interrupt the growth of less rapidly growing grains. The higher the rate of vertical growth is, the higher the probability of „survival" of such grain is.

Coatings D1−D3 are highly homogeneous, and imaging by the scanning electron microscope does not allow unambiguous determination of their crystal structure. Therefore, for a more detailed analysis of such coatings structure, the study was made with transmission electron microscope (Fig. 2).

As can be seen from the TEM images, the structure of the D1−D3 films (Fig. 2, f−h) contains both separate ultrananosized diamond crystals (size $\sim 5$ nm) and dendritic diamond clusters. The length of the dendrites ranges from tens to several hundreds of nanometers. Such pattern of growth indicates that during synthesis the films undergo constant active renucleation, which simultaneously ensures the formation of ultra-small diamond crystals and provokes the formation of crystalline clusters with a complex shape, nonrelevant in MCD and NCD structures. The papers [38,39] described the mechanism of growth of dendritic clusters in UNCD films. The fastest growth of nuclei occurs in the crystallographic direction (100), which ensures the vertical growth of clusters, while the (111) faces,

due to structural defects, become sites for the formation of secondary diamond nuclei. The process of their growth proceeds in the same way. As a result, the process of formation of dendritic clusters leads to the formation of a spherical structure observed on the film surface. Significant differences in the structure of films D1−D3 were not revealed.

The data of the electron diffraction patterns (Fig. 2, inserts) confirm the polycrystalline nature of all synthesized diamond films with diamond lattice planes identified as (111), (220), (311). For MCD film the diffraction pattern is a combination of typical single- and polycrystalline patterns, i.e. both the lattice in the form of individual dots and diffusion rings are observed. The diffraction patterns for films D1−D3 are typical for polycrystalline materials with small crystal sizes. In this case, as the concentration of methane in the gas phase increases, the homogeneity of the diffraction rings increases, which indicates the decrease in the size of diamond crystals.

The Raman spectra of all samples (Fig. 3) have five common peaks, among which there are two peaks of trans-polyacetylene (t-PA) Raman modes corresponding to the wave numbers $\sim 1146$ and $\sim 1460$ cm$^{-1}$ [42], the peak associated with the vibrational density of states (VDOS) of small diamond crystals or with diamond-like carbon ($d_{nc}$) $\sim 1235$ cm$^{-1}$ [43,44], peaks of disordered carbon (D-band) $\sim 1340$ cm$^{-1}$ and graphite structures (G-band) $\sim 1563$ cm$^{-1}$ [45]. The spectrum of the MCD sample also has the intense peak of diamond or $sp^3-$carbon corresponding to the wave number $\sim 1332$ cm$^{-1}$ [46], which indicates the microcrystalline nature of the diamond film. The spectra of samples D1−D3 clearly show two peaks of trans-polyacetylene, the presence of which is considered characteristic of diamond nanocrystalline structures [42]. When analyzing the spectra of the samples D1−D3, no peak was detected at $\sim 1332$ cm$^{-1}$, which is associated with high full width at half-maximum (FWHM) value for crystals with small sizes. Besides, the relative intensity of
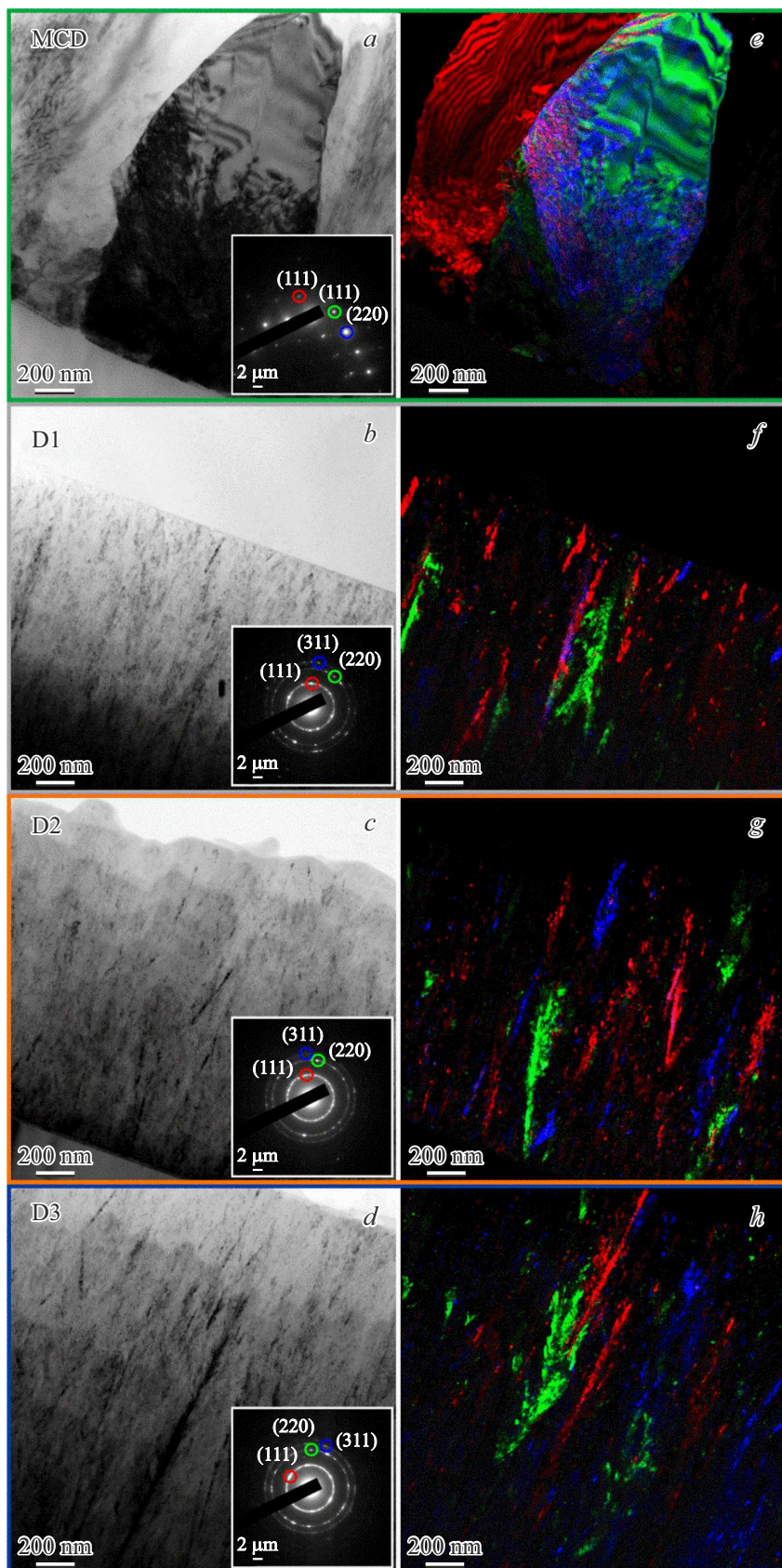
**Figure 2.** Bright-field TEM images of films (*a*−*d*), corresponding SAED patterns (on insets), dark-field TEM images from selected reflections (*e*−*h*).
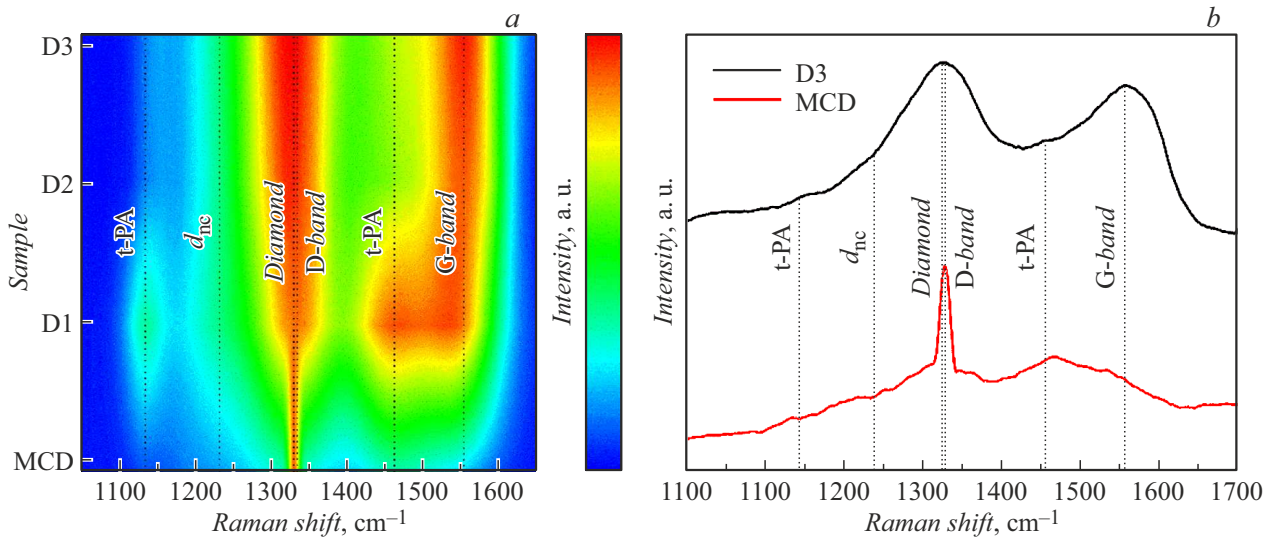
**Figure 3.** Map of Raman spectra of synthesized films (*a*), Raman spectra of films deposited at the maximum and minimum concentrations of $CH_4$ (*b*).

the peak of $sp^2$−carbon (D-band) in the film composition is much higher than that of $sp^3$− carbon [47]. Spectral patterns of samples D1−D3 are typical for UNCD films [48,49]. For all samples with the methane concentration increasing in the working gas during deposition, there is a trend towards the intensity increasing of the peaks of amorphous carbon (D-band) and graphite domains (G-band).

The X-ray diffraction spectra (Fig. 4) contain peaks at $2\Theta \sim 43.8°$, $75.6°$ and $91.6°$, which corresponds to the diamond lattice planes (111), (220), and (311). These data correlate with the TEM data of electron diffraction patterns. As the methane concentration in the gas phase increases, the full width at half-maximum (FWHM) increases, which indicates the crystallinity decreasing of the films. The calculation by the Scherrer formula was carried out in order to estimate the size of crystals (1) [50].

$$D = \frac{K \cdot \lambda}{\beta \cdot \cos \Theta},\qquad(1)$$

where $D$ — average crystal size, $K$ — Scherrer constant, $\lambda$ — X-ray wavelength, $\beta$ — peak width at half height and $\Theta$ — diffraction angle.

The average calculated crystal size of films D1−D3 for all growth orientations was 6.5, 5.5, and 4.5 nm, respectively.

The hardness and modulus of elasticity of the synthesized samples were measured (Fig. 5). It follows from the graph that the mechanical properties of diamond films have an inverse dependence on the concentration of $CH_4$ in the gas phase during deposition. Thus, the MCD film has the highest values of hardness and modulus of elasticity, equal to 95.15 and 974.5 GPa, respectively. These values are closest to single-crystal diamond [51,52]. With the increase in the methane concentration, the mechanical properties of the films decrease, since the volume of non-diamond phases, which have significantly lower physical and mechanical

parameters, increases in the composition of the films. Film D1 has the highest values of hardness and modulus of elasticity among samples with dendritic structure, equal to 87 and 891 GPa, respectively. The lowest values were obtained for sample D3, equal to 50.4 and 520 GPa, for hardness and modulus of elasticity, respectively. For sample D2, the ratio of hardness to the modulus of elasticity ($H/E$) $> 0.1$ is observed, which theoretically indicates a better load distribution over the area and high crack resistance [53,54]. The trend towards the decrease in hardness and modulus of elasticity with grain size decreasing is also traced in other papers [19,21,23,26]. The values of hardness and modulus of elasticity in the paper [21] are in the range of 68 to 86 GPa and of 597 to 857 GPa, respectively, for NCD films (crystal size of 9 to 60 nm). The paper [23] presents values for UNCD (crystal size ~2.7 nm) equal to 29 and 225 GPa for hardness and modulus of elasticity, respectively. The values of the mechanical properties of nanocrystalline films (crystal size 15.2−19 nm) in the paper [19] are comparable with those measured in the present paper. The hardness and modulus of elasticity of the films, measured in the paper [26], have comparable values with samples D1 and D2. The comparison of the results shows that the mechanical properties of the synthesized diamond films with dendritic structure correlate with the data of other papers.

The residual stresses in the films after deposition were calculated using the Stoney equation (3) in order to evaluate the adhesion of the coatings to the substrate. The calculation took into account the influence of the coating thickness and composition of the gas phase during deposition on the level of residual stresses. For the calculation by the Stoney formula, the biaxial moduli of elasticity of the substrate and coating were preliminarily calculated according to (2):

$$M = \frac{E}{(1 - \nu)},\qquad(2)$$
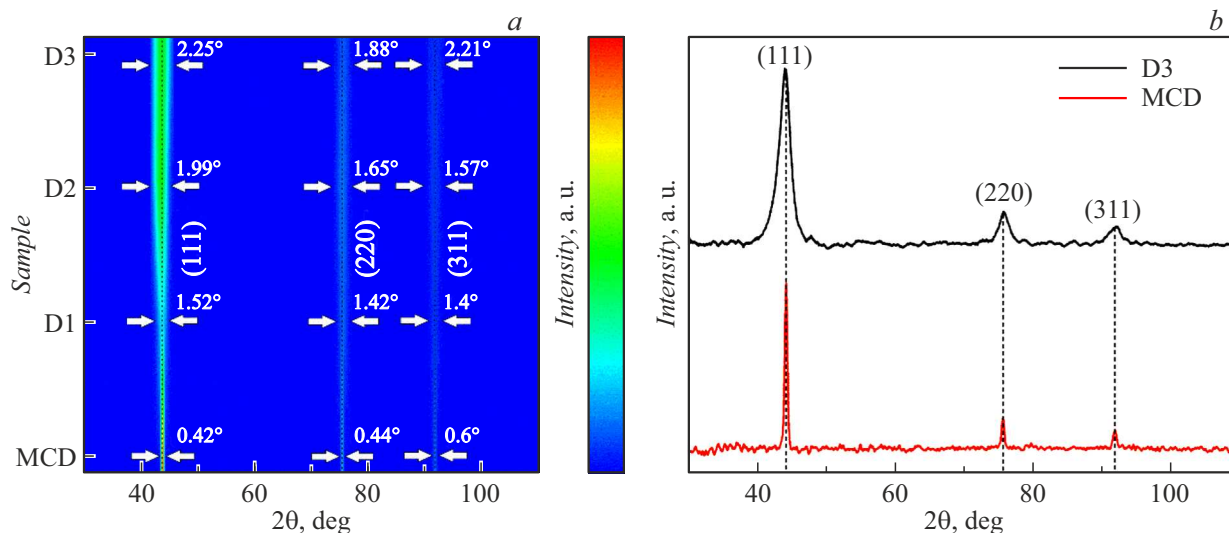
**Figure 4.** Measurement map of X-ray diffraction analysis of the synthesized films (*a*), X-ray spectra of films grown at the maximum and minimum concentrations of CH$_4$ (*b*).
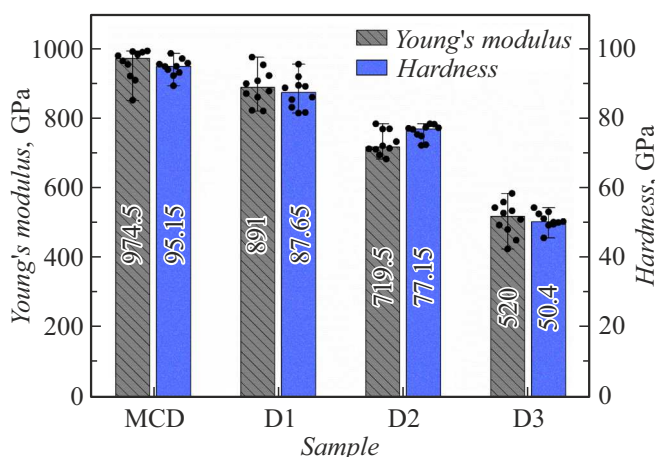


**Figure 5.** Hardness and modulus of elasticity of synthesized diamond films; the dots on the graph mark the measured values, the columns — the calculated median values.

where $M$ — biaxial modulus of elasticity, $E$ — modulus of elasticity, $\nu$ — Poisson's ratio.

The modulus of elasticity and Poisson's ratio of the substrate are 179 GPa [55] and 0.28 [56], respectively. The calculations of the biaxial modulus of elasticity of the coating considered the measured values of the modulus of elasticity (shown in Fig. 5). The Poisson's ratio of the microcrystalline film is 0.0791 [57], while the same of the ultrananocrystalline film is 0.201 [20]:

$$\sigma_f = M_s \frac{t_s^2}{6t_f}\left(\frac{1}{R} - \frac{1}{R_0}\right)\left[1 + \frac{t_f}{t_s}\left(\frac{4M_f}{M_s} - 1\right)\right], \quad (3)$$

where $\sigma_f$ — residual stresses, $M_s$ and $M_f$ — biaxial moduli of elasticity of the substrate and coating, respectively, $t_s$ and $t_f$ — thickness of the substrate and coating, respectively,

$R_0$ — radius of curvature of the substrate before deposition, $R$ — is the radius of curvature of the coated substrate.

Since the deposition process in the CVD method is carried out at sufficiently high temperatures, the substrate and the coating deform differently during cooling due to the difference in thermal expansion coefficients. The stresses formed in this case affect the adhesion of the coating to the substrate, i.e. the higher the stress level is, the lower the adhesion is. Fig. 6 shows a graph of the calculated residual stresses in the synthesized films (Fig. 6,*a*) and schematic examples of samples with tensile and compression residual stresses (Fig. 6,*b,c*).

It can be seen from the graph (Fig. 6,*a*) that MCD films experience the highest compression stresses in modulus, they increase with the increase in the coating thickness from $-0.408$ to $-0.482$ GPa. Films D1 and D2 change the nature of residual stresses from compression to tensile with the coating thickness increasing. The total stress values of these films are the smallest of all samples. Film D3 has tensile stresses with values in the region of $0.144-0.174$ GPa.

The surface profiles of the samples were obtained, and the surface roughness values were measured (Fig. 7) depending on the composition of the working gas and the film thickness. From the graph (Fig. 7,*a*) the difference in the level of roughness of the MCD and UNCD films is obvious. The measured roughness of samples of the MCD series depending on the film thickness ranges from 94.7 to 157.1 nm. The smallest roughness for UNCD samples was measured for sample D3, having thickness of $\sim 5\,\mu$m, and equals to 9.6 nm, and $\sim 11\,\mu$m, and equals to 16.4 nm. As compared with ultrananocrystalline samples the microcrystalline samples show by an order of magnitude higher values of roughness. For all samples, the following dependences are retained: the roughness increases with the film thickness increasing; and decreases with the methane
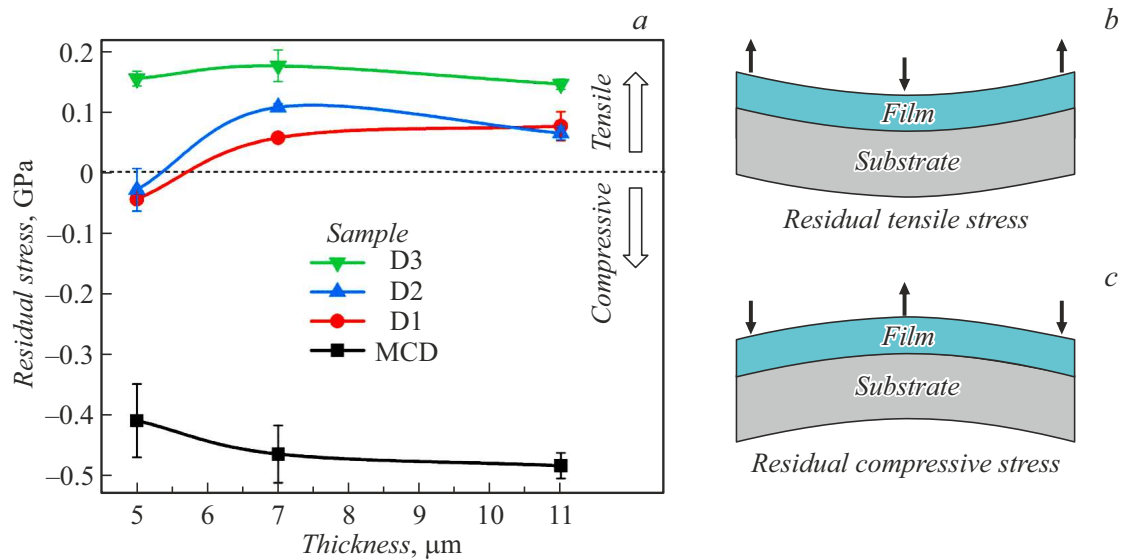
**Figure 6.** Diagram of residual stresses of diamond films vs. the thickness (*a*), schematic examples of samples with tensile (*b*) and compression (*c*) stresses.
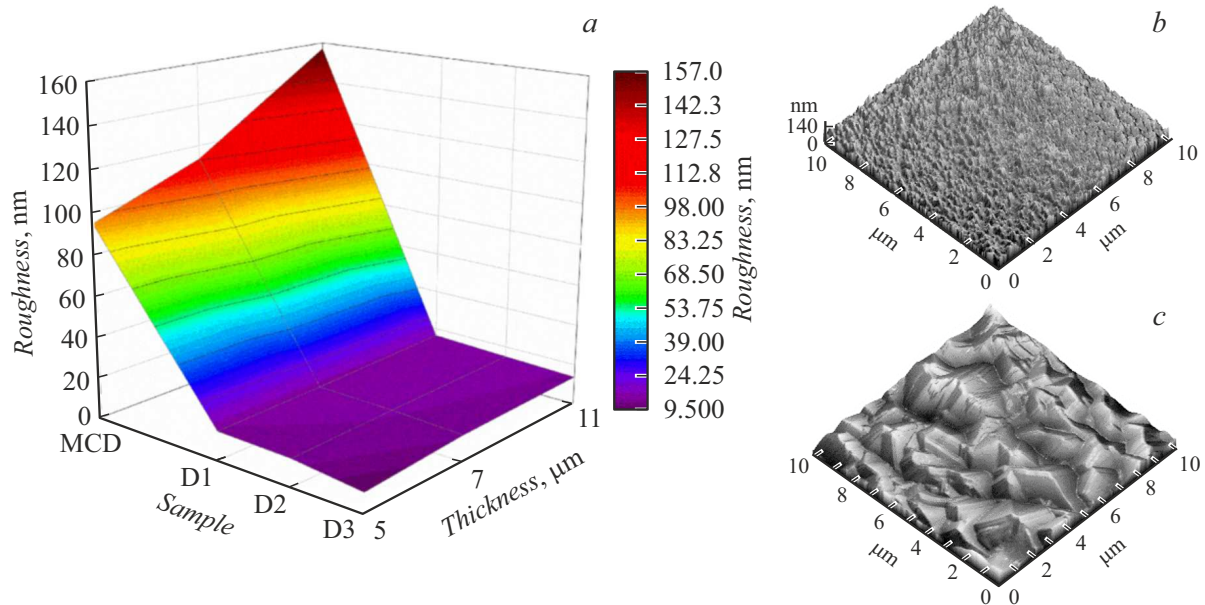


**Figure 7.** Map of the surface roughness of the synthesized samples vs. film thickness (*a*); AFM profiles of the sample surface with the lowest (*b*) and highest (*c*) roughness.

concentration increasing in the gas phase during deposition. Comparison of surface morphology data with other papers shows that the surface roughness of MCD films coincides with the results obtained by other authors [26,30], and the roughness of films D1−D3 is lower than for NCD films [19,21] even at a greater thickness, and is on the same level with the values of UNCD films [23,30,58], while in the present paper the roughness dependence on the UNCD films thickness is traced, which was not reported in other papers.

## Conclusion

The paper presents the results of study of structural transformations and changes in the mechanical properties of diamond films synthesized by the HFCVD method with the change in the methane concentration in the atmosphere $H_2/CH_4$. The results of the microstructure analysis of the samples grown at high methane concentrations (12.2−19.3 vol.%) by the TEM method showed that the films synthesized under such deposition conditions have the

dendritic structure, while their spectra of Raman scattering, X-ray spectra, and also electron diffraction patterns are typical for ultrananocrystalline diamond films. The dynamics of changes in hardness and modulus of elasticity in films with the change in the methane concentration in the working gas is shown. The highest measured values were obtained for the microcrystalline film and were equal to 95.15 and 974.5 GPa for hardness and modulus of elasticity, respectively. The values of hardness and modulus of elasticity of ultrananocrystalline films range from 50.4 and 520 GPa to 87 and 891 GPa, respectively, i.e. the difference between micro- and ultrananocrystalline films ranges from 10 to 47%. Residual stresses in microcrystalline films are of compressive nature and, depending on the film thickness, range from 0.408 to 0.482 GPa. With the methane concentration increasing, the increase in tensile stresses is observed. The highest stresses by modulus in ultrananocrystalline films are tensile stresses and range from 0.144 to 0.174 GPa, depending on the thickness. The surface morphology changes significantly upon transition from micro- to ultrananocrystalline structure. The roughness values increase with the increase in the film thickness and with the decrease in the concentration of $CH_4$ in the working gas. Depending on the thickness, the surface roughness of microcrystalline films ranges from 94 to 157 nm. Roughness values in ultrananocrystalline films range from 9 to 16 nm depending on thickness and methane concentration. In this case, the change in the surface roughness of ultrananocrystalline films is in the range of 30% with the methane concentration increasing from 12.2 to 19.3 vol.%.

## Funding

## Conflict of interest

The authors declare that they have no conflict of interest.

## References

[1] E. Wilks, J. Wilks, *Properties and Applications of Diamond* (Butterworth-Heinemann, Oxford, 1994)

[2] R.S. Balmer, J.R. Brandon, S.L. Clewes, H.K. Dhillon, J.M. Dodson, I. Friel, P.N. Inglis, T.D. Madgwick, M.L. Markham, T.P. Mollart, N. Perkins, G.A. Scarsbrook, D.J. Twitchen, A.J. Whitehead, J.J. Wilman, S.M. Woollard. J. Phys.: Condensed Matter., **21** (36), 364221 (2009). DOI: 10.1088/0953-8984/21/36/364221

[3] S.E. Coe, R.S. Sussmann. Diamond and Related Mater., **9**, 1726 (2000). DOI: 10.1016/S0925-9635(00)00298-3

[4] T.A. Scott. Adv. Appl. Ceramics, **117** (3), 161 (2017). DOI: 10.1080/17436753.2017.1389462

[5] S.E. Grillo, J.E. Field. Wear, **254** (10), 945 (2003). DOI: 10.1016/S0043-1648(03)00297-7

[6] I.P. Hayward, I.L. Singer, L.E. Seitzman. Wear, **157** (2), 215 (1992). DOI: 10.1016/0043-1648(92)90063-E

[7] H. Sein, W. Ahmed, M. Jackson, R. Woodwards, R. Polini. Thin Solid Films, **447**, 455 (2003). DOI: 10.1016/j.tsf.2003.08.044

[8] G. Zhao, Z. Li, M. Hu, L. Li, N. He, M. Jamil. Diamond and Related Mater., **100**, 107589 (2019). DOI: 10.1016/j.diamond.2019.107589

[9] F.A. Almeida, J. Sacramento, F.J. Oliveria, R.F. Silva. Surf. Coatings Technol., **203**, 271 (2008). DOI: 10.1016/j.surfcoat.2008.08.075

[10] O. Auciello, A.V. Sumant. Diamond and Related Mater., **19**, 699 (2010). DOI: 10.1016/j.diamond.2010.03.015

[11] D. Guo, N. Cai, G. Wu, F. Xie, S. Tan, N. Jiang, H. Li. Appl. Sci., **10** (17), 6090 (2020). DOI: 10.3390/app10176090

[12] R.J. Nemanich, J.A. Carlisle, A. Hirata, K. Haenen. MRS Bulletin, **39** (6), 490 (2014). DOI: 10.1557/mrs.2014.97

[13] A. Gicquel, K. Hassouni, F. Silva, J. Achard. Current Appl. Phys., **1** (6), 479 (2001). DOI: 10.1016/S1567-1739(01)00061-X

[14] C.J. Widmann, W. Müller-Sebert, N. Lang, C.E. Nebel. Diamond and Related Mater., **64**, 1 (2016). DOI: 10.1016/j.diamond.2015.12.016

[15] X. Jia, N. Huang, Y. Guo, L. Liu, P. Li, Z. Zhai, B. Yang, Z. Yuan, D. Shi, X. Jiang. J. Mater. Sci. Technol., **34** (12), 2398 (2018). DOI: 10.1016/j.jmst.2018.04.021

[16] O. Auciello. Functional Diamond, **2** (1), 1 (2022). DOI: 10.1080/26941112.2022.2033606

[17] M. Salgado-Meza, G. Martínez-Rodríguez, P. Tirado-Cantú, E.E. Montijo-Valenzuela, R. Garcia-Gutierrez. Appl. Sci., **11** (18), 8443 (2021). DOI: 10.3390/app11188443

[18] R. Rani, K. Panda, N. Kumar, A.T. Kozakov, V.I. Kolesnikov, A.V. Sidashov, I-N. Lin. Scientific Reports, **8** (1), 283 (2018). DOI: 10.1038/s41598-017-18425-4

[19] G. Yan, Y. Wu, D. Cristea, L. Liu, M. Tierean, Y. Wang, F. Lu, H. Wang, Z. Yuan, D. Munteanu, D. Zhao. Appl. Surf. Sci., **494**, 401 (2019). DOI: 10.1016/j.apsusc.2019.07.110

[20] M. Mohr, A. Caron, P. Herbeck-Engel, R. Bennewitz, P. Gluche, K. Brühne, H.-J. Fecht. J. Appl. Phys., **116**, 124308, (2014). DOI: 10.1063/1.4896729

[21] M. Wiora, K. Brühne, A. Flöter, P. Gluche, T.M. Willey, S.O. Kucheyev, A.W. Van Buuren, A.V. Hamza, J. Biener, H.-J. Fecht. Diamond and Related Mater., **18** (5−8), 927 (2009). DOI: 10.1016/j.diamond.2008.11.026

[22] A.V. Sumant, O. Auciello, A. Krauss, D.M. Gruen, D. Ersoy, J. Tucek, A. Jayatissa, E.A. Stach, N. Moldovan, D.C. Mancini, H.-G. Busmann, E.M. Meyer, Mater. Res. Society Sympos. Proceed. Materi. Res. Society, **657** (2000). DOI: 10.1557/PROC-657-EE5.33

[23] B. Shen, Q. Lin, S. Chen, Z. Ji, Z. Huang, Z. Zhang. Surf. Coatings Technol., **378**, 124999 (2019). DOI: 10.1016/j.surfcoat.2019.124999

[24] E. Salgueiredo, M. Amaral, F.A. Almeida, A.J.S. Fernandes, F.J. Oliveira, R.F. Silva. Surf. Coatings Technol., **236**, 380 (2013). DOI: 10.1016/j.surfcoat.2013.10.017

[25] E.L.H. Thomas, G.W. Nelson, S. Mandal, J.S. Foord, O.A. Williams. Carbon, **68**, 473 (2014). DOI: 10.1016/j.carbon.2013.11.023

[26] H. Wang, C. Wang, X. Wang, F. Sun. Surf. Coatings Technol., **409**, 126839 (2021). DOI: 10.1016/j.surfcoat.2021.126839

[27] R. Zhang, Y. Zheng, J. Liu, C. Li, C. Chen, X. Hu, J. Li, R. Liu, H. Ye. Functional Diamond, **2** (1), 204 (2022). DOI: 10.1080/26941112.2022.2157225

[28] S. Tipawan Khlayboonme, Warawoot Thowladda. Key Engineer. Mater., **831**, 127 (2020). DOI: 10.4028/www.scientific.net/KEM.831.127

[29] M. Mertens, I.-N. Lin, D. Manoharan, A. Moeinian, K. Brühne, H.J. Fecht. AIP Adv., **7**, 015312 (2017). DOI: 10.1063/1.4975226

[30] V.S. Sedov, A.K. Martyanov, A.A. Khomich, S.S. Savin, E.V. Zavedeev, V.G. Ralchenko. Diamond and Related Mater., **109**, 108072 (2020). DOI: 10.1016/j.diamond.2020.108072

[31] Q. Lin, S. Chen, Z. Ji, Z. Huang, Z. Zhang, B. Shen. Surf. Coatings Technol., **419**, 127280 (2021). DOI: 10.1016/j.surfcoat.2021.127280

[32] O.A. Williams, M. Nesladek, M. Daenen, S. Michaelson, A. Hoffman, E. Osawa, K. Haenen, R.B. Jackman. Diamond and Related Mater., **17** (7-10), 1080 (2008) DOI: 10.1016/j.diamond.2008.01.103

[33] K.J. Sankaran, J. Kurian, H.C. Chen, C.L. Dong, C.Y. Lee, N.H. Tai1, I.N. Lin. J. Phys. D: Appl. Phys., **45** (36), 365303 (2012). DOI: 10.1088/0022-3727/45/36/365303

[34] E. Amonoo, V. Jha, T. Thornton, F.A. Koeck, R.J. Nemanich, T.L. Alford, Diamond and Related Mater., **135**, 109832 (2023). DOI: 10.1016/j.diamond.2023.109832

[35] R.W. Thoka, S.J. Moloi, S.C. Ray, W.F. Pong, I.-N. Lin. J. Electron Spectr. Related Phenomena, **242**, 146968 (2020). DOI: 10.1016/j.elspec.2020.146968

[36] B.-K. Song, H.-Y. Kim, K.-S. Kim, J.-W. Yang, N.-M. Hwang. Materials, **14** (2), 426 (2021). DOI: 10.3390/ma14020426

[37] J.-W. Park, K.-S. Kim, N.-M. Hwang. Carbon, **106**, 289 (2016). DOI: 10.1016/j.carbon.2016.05.035

[38] A. Zolotukhin, P.G. Kopylov, R.R. Ismagilov, A.N. Obraztsov. Diamond and Related Mater., **19** (7−9), 1007 (2010). DOI: 10.1016/j.diamond.2010.03.005

[39] A.A. Zolotukhin, M.A. Dolganov, A.N. Obraztsov. Diamond and Related Mater., **37**, 64 (2013). DOI: 10.1016/j.diamond.2013.04.003

[40] H. Zeng, N. Moldovan, G. Catausan. Diamond and Related Mater. **91**, 165 (2019). DOI: 10.1016/j.diamond.2018.11.016

[41] A. van der Drift. Phillips Research Reports, **21**, 267 (1967).

[42] H. Kuzmany, R. Pfeiffer, N. Salk, B. Günther. Carbon, **42** (5−6), 911 (2004). DOI: 10.1016/j.carbon.2003.12.045

[43] S. Prawer, K.W. Nugent, D.N. Jamieson, J.O. Orwa, L.A. Bursill, J.L. Peng. Chem. Phys. Lett., **332** (1−2), 93 (2000). DOI: 10.1016/S0009-2614(00)01236-7

[44] S. Prawer, R.J. Nemanich. Raman Spectroscopy of Diamond and Doped Diamond, Philosophical Transactions of The Royal Society A Mathematical Physical and Engineering Sciences, **362** (1824), 2537 (2004). DOI: 10.1098/rsta.2004.1451

[45] A.C. Ferrari, J. Robertson. Phys. Rev. B, **61** (20), 14095 (2000). DOI: 10.1103/PhysRevB.61.14095

[46] D.S. Knight, W.B. White. J. Mater. Res., **4**, 385 (1989). DOI: 10.1557/JMR.1989.0385

[47] P.C. Redfern, D.A. Horner, L.A. Curtiss, D.M. Gruen. J. Phys. Chem., **100**, 11654 (1996). DOI: 10.1021/jp953165g

[48] J. Birrell, J.E. Gerbi, O. Auciello, J.M. Gibson, J. Johnson, J.A. Carlisle. Diamond and Related Mater., **14** (1), 86 (2005). DOI: 10.1016/j.diamond.2004.07.012

[49] F. Klauser, D. Steinmüller-Nethl, R. Kaindl, E. Bertel, N. Memmel. Chem. Vapor Deposition, **16** (4−6), 127 (2010). DOI: 10.1002/cvde.200906827

[50] A. Heiman, E. Lakin, E. Zolotoyabko, A. Hoffman. Diamond and Related Mater., **11** (3), 601 (2002). DOI: 10.1016/S0925-9635(01)00631-8

[51] J.L. Lyu, S.-L. Wang, W. Bo, K. Nishimura, N. Jiang. Surf. Engineer., **35** (1), 1 (2018). DOI: 10.1080/02670844.2018.1447270

[52] Q.L. Wei, X.B. Yue, X.Y. Li, B. Liu, X.F. Zhang, D.J. Lei, Adv. Mater. Res., **1120**−**1121**, 378 (2015). DOI: 10.4028/www.scientific.net/AMR.1120-1121.378

[53] J. Blažek, J. Musil, P. Stupka, R. Čerstvý, J. Houška. Appl. Surf. Sci., **258** (5), 1762 (2011). DOI: 10.1016/j.apsusc.2011.10.039

[54] J. Musil. Surf. Coat. Technol., **207**, 50 (2012). DOI: 10.1016/j.surfcoat.2012.05.073

[55] B. Bhushan, X. Li. J. Mater. Res., **12** (1), 54 (1997). DOI: 10.1557/JMR.1997.0010

[56] M.A. Hopcroft, W.D. Nix, T.W. Kenny. J. Microelectromechan. Systems, **19** (2), 229 (2010). DOI: 10.1109/JMEMS.2009.2039697

[57] C.A. Klein, G.F. Cardinale. Diamond and Related Mater., **2** (5−7), 918 (1993). DOI: 10.1016/0925-9635(93)90250-6

[58] W. Kulisch, C. Popov, T. Sasaki, L. Sirghi, H. Rauscher, F. Rossi, J.P. Reithmaier. Phys. Status Solidi (A) Applications and Mater., **208** (1), 70 (2011). DOI: 10.1002/pssa.201026066

*Translated by I.Mazurov*